3D fractal analysis of multi-scale morphology of sand particles with μCT and interferometer

Hong-Wei Yang[1,2], Sérgio D.N. Lourenço[3], Béatrice A. Baudet[4,*]

[1] *Institute for Geology, Mineralogy, and Geophysics, Ruhr-University Bochum, Bochum, 44801 Germany*

[2]*International Joint Research Laboratory of Henan Province for Underground Space Development and Disaster Prevention, Henan Polytechnic University, Jiaozuo 454003, China*

[3]*Department of Civil Engineering, The University of Hong Kong, Pokfulam Road, Hong Kong*

[4]*Department of Civil, Environmental and Geomatic Engineering, University College London, London, Gower Street, LondonWC1E 6BT, UK*

Revised manuscript submitted to

Géotechnique

On

30/08/2019

for possible publication

[*]Corresponding author; email: b.baudet@ucl.ac.uk

Abstract: The particle morphology of granular materials comprises different characteristic scales, including particle shape and surface texture. Different methods have been proposed to characterise the morphology using three-dimensional parameters, among which is the fractal method. These methods, however, are applied either at the scale of particle shape or surface texture. A framework unifying the multi-scale morphology obtained from different measuring instruments could advance the current understanding into this topic, but is still lacking. This paper proposes a novel methodology to characterise the morphology of sand particles across different scales based on results from two previously adopted instruments with different measuring capabilities - an X-ray micro-computed tomography (μCT) and a high-resolution optical microscope equipped with an interferometer. The methodology is applied to sand-sized particles of a crushed granitic rock and a natural quarzitic sand (Fujian sand). By using spectrum analysis on data from both μCT and interferometer measurements, a single fractal dimension is found linking the spectrum of the two measurements for the crushed granitic rock. For Fujian sand, two self-affine patterns are observed, which serves as a separation between particle shape and surface texture and also indicates that the fractal dimension obtained at larger scale may not be simply extended to small scales. The translation of surface measurements into numerically reconstructed particle morphology at particle shape and surface texture scale is demonstrated by using spherical harmonic expansion and power spectral density functions.

Keywords: fractals; microscopy; sands

1. Introduction

The morphology of soil grains is conventionally described at different characteristic scales, such as particle shape and surface texture. In general, particle shape describes the overall particle form and roundness of corners, while surface texture describes the small surface features, such as local curvature and surface roughness. Both particle shape and surface texture can have a significant effect on soil behaviour: for example, particle shape has been found to be influential to the critical state, dilation and hydraulic behaviour of granular materials (e.g. Carrier, 2003; Cho et al. 2006; Matsushima and Chang, 2011; Yang et al., 2014; Yang and Luo 2015), and surface texture is strongly related to the contact stiffness and inter-particle coefficient of friction (e.g. Senetakis et al., 2013; Otsubo et al., 2015; Sandeep et al., 2018). Although with advanced technology it is now possible to measure the shape and surface texture of small-sized grains, the challenge of having a comprehensive description of the soil particle morphology across the scales, i.e. from surface texture to shape, remains. It is in particular not clear whether, and how, the particle shape and surface texture may be related.

The shape and surface texture of soil grains reflect their past history but whether they are linked is not clear. If Fourier series are used to describe the morphology of particles (as in e.g. Bowman et al., 2001), the surface roughness, at one extreme of the morphology scale, is governed by high-order harmonics, opposite to the particle shape analysis, at the other extreme of the scale, which is provided by the lower harmonics (Orford & Whalley, 1987). Particle shape and surface roughness have so far been investigated separately because no existing technology can span the range of both scales. The techniques of micro Computed Tomography (μCT) and 3D laser scanner, used to investigate grain shape, are now commonly used by anyone interested in the

microstructure of granular soils, but they are known for not giving quantitative descriptions of particle morphology, and their output, either a series of pictures or point clouds, needs to be processed to yield any usable result. Similarly, the interferometer, used to quantify the roughness of soil particles, gives a surface topography as a function of sample height at discrete points, and although a simple statistical parameter (e.g. S_q) can be obtained by a simple calculation, an advanced analysis is required to reveal more features of the surface texture. Even in studies where both the shape and surface roughness of sand grains were investigated, e.g. in Alshibli et al. (2014), different processes were used to analyse the data obtained from distinct apparatuses.

Researchers who have tried to link the two scales, through fractal analysis of the grain perimeter for example, have concluded from a limited number of analyses that there may be two separate fractal elements, a textural fractal and a structural fractal (Orford & Whalley, 1987), but the intersection between the two domains has not been solved, nor the existence of the two domains been substantiated by additional data. The work presented in this paper proposes that a single method to analyse the data from distinct apparatuses for shape and surface roughness can be adopted so that they can be interpreted within a unique framework.

Different characterisation methods have been proposed for particle morphology, but they are limited to either particle shape scale, (e.g. Garboczi, 2002; Zhou et al., 2015; 2018 and Zhao et al., 2016) or surface texture scale (e.g. Altuhafi et al., 2011; Alshibili et al., 2014; Yang et al., 2016; 2019). Parameters based on three-dimensional particle morphology have generally been favoured to describe soil grains in comparison to 2D parameters which are heavily dependent on the particle projection (e.g. Fonseca et al., 2012; Alshibli et al., 2014). Three-dimensional morphological measurements have been made with advanced instruments such as 3D laser scanners, μCT and optical

microscopes; for example, the μCT has been used to study the morphological features of either single particles (Zhao and Wang, 2016) or a granular assemblage (Fonseca et al., 2012), in which a stack of images was obtained and image processing technique was used to obtain the morphological features. Yet due to the limited voxel size or resolution of the obtained images, the obtained morphological features are usually limited to the particle shape scale. On the other hand, optical microscopes have been shown able to reveal the surface texture of sand down to the nanometre scale (e.g. Altuhafi et al., 2011; Alshibili et al., 2014; Yang et al., 2016; Yao et al., 2018).

For particle morphology at the particle shape scale, mathematical methods, such as spherical harmonic expansion method, (e.g. Garboczi, 2002; Zhou et al., 2015; 2018) or level-set method (Kawamoto et al., 2016) have been applied. For particle morphology at the surface texture scale, a statistical parameter, the root-mean-square value of the surface height to a mean plane (S_q), has been traditionally used (e.g. Altuhafi et al., 2011; Alshibili et al., 2014), although it does not enable a full reconstruction of the surface texture. Other approaches based on fractal analysis have been applied to try to characterise particle morphology across the scales, but this has been achieved at different, not overlapping scales so far. Zhou et al. (2018) derived a fractal dimension from μCT measurements that was obtained from the particle geometry and had to extrapolate to describe surface texture for implementing in a discrete element model. At the surface texture scale, fractal parameters have been used to reconstruct the surface texture (Yang et al., 2016; 2019).

This paper proposes a novel methodology to quantify the morphology of soil grains from nano- to micro-scale in three steps, which would be particularly useful to researchers modelling at the particle scale. First, the 3D particle morphology of sand is examined at the two scales by using X-ray micro Computed Tomography (μCT) and a

high-resolution optical microscope equipped with a white light interferometer. Then, it is proposed to link the surface measurements from μCT and interferometer by using spectrums in which the spherical harmonic expansion and Fourier transform are involved. This is followed by carrying out a fractal analysis of the spectra. An example has been included to demonstrate how the particle morphology measurements could be translated into a numerically reconstructed particle.

2. Tested sand and testing instruments

2.1 Tested sand

Two sands of different shapes and similar sizes were used: 1. Particles made of crushed granitic (CG) rock, which are mostly angular (Fig. 1a), and of which the surface texture has been successfully analysed by Yang et al. (2019). The parent rock is of grade II in the classification for rock material weathering grades, with soil being a grade VI material and fresh rock a grade I. A grade II granite is defined as 'fresh rock colours generally retained but stained near joint surfaces' (GEO, 2017). 2. Fujian sand (FS) (China ISO standard sand), which is a natural sand with a silica content of more than 98% that is mostly sub-rounded (Fig. 1b). Grain sizes of 0.6 to 2 mm and 1.18 to 2 mm of each sand were randomly selected for testing. In total, more than 68 particles for crushed granitic rocks and 50 particles for Fujian sand were tested.

2.2 Testing instruments

The particles were scanned using an X-ray μCT scanner (Toscaner-3000, Toshiba, Japan). They were held in fixed positions by placing in a cylindrical container of diameter 20 mm filled with silica oil during scanning. Particles were arranged to be separate from each other (Fig. 1) so that over-segmentation of particles is avoided in the image processing. A voxel size ranging from 15.5 μm to 18.5 μm was achieved.

Processing of the obtained images is briefly introduced and includes the following steps: a) to reduce noise in the raw images, a filter of size 3 x 3 x 3 was used (Gozalez and Woods, 2010). b) to separate the solid phase (sand particles) from void space and silicone oil, the method of Otsu (1979) embedded in the image-processing package-ImageJ (Rasband, 1997-2011) was used to obtain the threshold value (Fonseca et al., 2012). One of the built-in plug (3D segmentation) enables the solid phase of each particle to be labelled with a numeric. c) The voxel assemblage representing each particle was then smoothed using a 3D Gaussian filter with a kernel size of five voxels, leading to a smoothed 3D matrix of scalar values (Zhou et al., 2018). d) Surface reconstruction was then performed based on the smoothed 3D matrix so that it is represented by a triangulated mesh (specified by a face list and a vertex list). Intrinsic MATLAB functions of smooth3 and isosurface were applied in steps c and d. The reconstructed surface for each particle was finally used for further analysis.

The surface features were examined using an optical microscope with white light interferometry (M3D 3000, Fogale Nanotech, France). The surface topography is described by an interferogram that is a function of the sample height at discrete points. The best in-plane (perpendicular to surface height) resolution is 0.184 μm and 3 nm resolution in the surface height direction, with the measuring area being up to 141.3 × 106.6 μm (Yang et al., 2016). From the optical interferometer, an open surface with a measuring area of 106.6× 106.6 μm was acquired, corresponding to 578×578 discrete points. Although the largest square measuring area has been used, the measuring area is small compared to the particle size. Three measurements were made per particle, following Yao et al.'s (2018) finding that for particle sizes of 1.18~2 mm, three measurements per particle can provide a reliable surface roughness value, as some

common features can be observed across the particle, such as v-shaped indents in the quarzitic Leighton Buzzard sand (Yang et al., 2016; Yao et al., 2018).

3. Test results and surface characterisation by power spectral density

We report results obtained with the two testing techniques, μCT and interferometer, which were both analysed by using power spectrum. Analysing data from these two techniques in the same framework is new, as they were developed, and are typically looked at, separately. For μCT measurements, only the surface points from a scanned particle are used and they constitute a closed surface. For interferometer measurements, the surface examined is an open surface and the local area is measured. It was therefore necessary to apply the power spectral density (PSD) functions slightly differently for the two measurements: using Fourier transform for the open surface, and spherical harmonics for the closed surface.

3.1 Power spectrum of μCT measurements

The first step in calculating the power spectrum of μCT measurements is the approximation of 3D particle surfaces by spherical harmonic (SH) functions. The SH functions have been widely used to approximate 3D particle surfaces (e.g. Garboczi, 2002; Zhou and Wang, 2017 and Zhou et al., 2018). In this study, the method proposed by Garboczi (2002) to reconstruct star-shaped particles was adopted. In the method, a unique pair of angles (θ, φ) (where θ is [0, π] and φ is [0, 2π]) was assigned to each point of the original particle surface, which is termed spherical parameterization. After spherical parameterization, the distance from the origin that is located inside a particle

or polar radius $r(\theta,\ \varphi)$ of each point on the original particle surface is expressed as an expansion of SH series and is given as:

$$r(\theta,\varphi)=\sum_{l=0}^{N}\sum_{m=-l}^{l} f_{lm}Y_l^m(\theta,\varphi) \tag{1}$$

where N is the maximal degree of the SH function, f_{lm} is the corresponding SH expansion coefficient and needs to be determined and Y_l^m is the spherical harmonic of degree l and order m which forms a complete set of orthonormal functions and is given (Condon-Shortley phase) as:

$$Y(\theta,\varphi)=\sqrt{\frac{2l+1}{4\pi}\frac{(l-m)!}{(l+m)!}}P_l^m(\cos\theta)e^{im\varphi} \tag{2}$$

where P_l^m is an associated Legendre function. Following Chevrot et al. (1998) and Wieczorek and Simons (2005), the angular harmonic degree is used.

Eq. (1) indicates that at the zero degree, the resulting particle shape is a sphere; the radius is the mean spherical harmonic radius (Wieczorek, 2015) and is given as:

$$r_{00}=\frac{f_{00}}{\sqrt{4\pi}} \tag{3}$$

Once the f_{lm} is determined (by using the least square method as in this study), the particle surface can be re-built. The surface of a unit sphere is firstly described by a geodesic polyhedron that made of triangles. A geodesic polyhedron with 10242 vertices and 20480 faces is a good approximation of a sphere (Mollon and Zhao, 2014). All the

angular coordinates angles (θ, φ) of these 10242 points are known as well as the f_{lm}, the polar radius can thus be determined by the inverse of Eq. (1). An example is given in figure 2. The particle surface becomes more detailed when a particle is reconstructed at an increasingly larger maximum harmonic degree. Starting from the degree of 1, the reconstructed shape becomes ellipsoid and then gradually irregular with increasing degree. Particles reconstructed at lower harmonic degrees are influenced significantly by the particle shape, as also observed in Zhou et al. (2018) and Su and Yan (2018). As the maximum degree increases, the particle is reconstructed at greater details and thus the reconstructed particle resembles more the original scanned particle.

At the same time, based on the triangulated surface meshes, the surface area and volume of reconstructed particle can be estimated, respectively, as (Zhou et al., 2018):

$$SA = \sum_i \frac{1}{2}\left|\overrightarrow{A_iB_i} \times \overrightarrow{B_iC_i}\right| \tag{4}$$

$$V = \sum_i \frac{1}{6}\left|\overrightarrow{OA_i} \cdot \left(\overrightarrow{OB_i} \times \overrightarrow{OC_i}\right)\right| \tag{5}$$

where O is the centre of the particle and A_i, B_i and C_i constitute the vertices of the ith face triangular of the surface mesh. The variation of particle surface area and volume with harmonic degree for selected particles is shown in figure 3. For particles reconstructed at a harmonic degree of 2, the difference in volume between reconstructed and scanned particles is within 20%, and for a harmonic degree greater than 8 the particle volume is almost as scanned (ratio more than 95%). The ratio in volume of reconstructed and scanned particle converges rapidly to unity whereas the rate of increase in the surface area is still non-negligible, as even at the degree of 18, the full

surface features as scanned could not be reproduced. Possible reasons include the overestimation of the surface area from i.e. the boundary detecting algorithm adopted for the image analysis (Fonseca, 2011; Zhou et al., 2018), or the underestimation of the surface area by the truncated harmonic function at an insufficiently large harmonic degree.

The power spectrum of the smooth function $r(\theta, \varphi)$ can then be obtained by taking a further step of SH analysis. The spectrum is calculated as a sum of individual contributions of different SH degree l and is given by e.g. Chevrot et al. (1998):

$$PSD(l) = \sum_{m=-l}^{l} \frac{|f_{lm}|^2}{2l+1} \tag{6}$$

As indicated by Eq. (6) the power spectrum contains a sum over all orders m and is invariant under a rotation of the coordinate system (Kaula, 1967). It generally reflects the proportion of spatial features at each harmonic degree. The whole particle surface can thus be regarded as the superposition of spatial features at each harmonic degree. Another advantage of using PSD is that it is directly related to the traditionally adopted parameter, S_q, square-root value of surface height to a mean plane, to describe surface texture through (e.g. Kaula, 1967; Bills and Kobrick, 1985):

$$S_q = \sqrt{\sum_{l=0}^{l_{max}} PSD(l)} \tag{7}$$

The equation shows that the S_q value increases with the maximum harmonic degree. It will be used in the rebuilding of particle surface at multi-scale morphology.

Figure 4 shows the power spectral density obtained from µCT measurements, where the PSD is plotted versus harmonic degree plane. The average value is also indicated to highlight the trend. A maximum harmonic degree of 18 is used here, that is at the same level as other researchers have used in particle shape reconstruction (i.e. 20 in Zhou et al., 2018). As a reminder, a low harmonic degree reflects the large spatial features (at large length scale) of the particle surface while a higher degree reflects the small spatial features. A jump is observed at a harmonic degree of 2, indicating the predominance of the particle shape (as also seen in Figure 2). For a harmonic degree greater than 2, the PSD decreases gradually.

3.2 Power spectrum of interferometer measurements

The power spectrum of the results from the interferometer measurements on an open surface has been given by Persson et al. (2005) which makes use of the discrete Fourier transform of surface heights:

$$PSD(k_x, k_y) = \frac{A}{\left(N_x N_y\right)^2} \frac{1}{\left(2\pi\right)^2} \left|2\mathrm{D}FFT\right|^2 \tag{8}$$

where A is the projection area of surface heights $h(x, y)$ and is equal to $N_x N_y a^2$ in which N_x, N_y are data points on the x and y direction and a is the resolution on the x-y plane. The 2D FFT can easily be calculated by built-in functions, such as fft2 in Matlab. A routine angular averaging, such as using the numerical recipe of Persson et al. (2005), can then be performed where the surface is assumed to be isotropic so that the PSD(**q**) reduces to PSD(q) and is independent of the x or y direction (Nayak,1971). Denoting the angular averaging by the symbol $\Im$, the one-dimensional PSD ($PSD_{Eq.7}$) is:

$$PSD(k)_{Eq.8} = \Im PSD(k_x, k_y) \tag{9}$$

Some test results from interferometer measurements are shown in figure 5 in which the surfaces of three particles are shown. Three measurements were performed on each particle, at three different locations. The surfaces measured at the different locations are not exactly the same. This is expected as it is usually assumed (and this is a basis for the PSD method) that surfaces are the result of random creation processes. The associated power spectrum is also shown (down-right subplot in each figure) in the PSD versus wavenumber plane. The wavenumber is inversely proportional to the wavelength (a larger wavenumber is related to the small length scale features, and vice versa). The power spectra for different measurements on the same particle are slightly shifted vertically but show no significant difference in the slope (difference of magnitude of 0.01). The roughness value for the local area, S_q, which can be obtained from the PSD as follows (Persson, 2005):

$$S_q = \left(2\pi \int_{q_c}^{q_1} PSD(q) q \mathrm{d}q\right)^{0.5} \tag{10}$$

where q_1 is the largest wavenumber and relates to the resolution on horizontal plane of the interferometer and q_0 is the smallest wavenumber, is more affected but the order of magnitude is unchanged.

Figure 6 shows all the interferometer results in the PSD versus wavenumber plane. No spike or jump is observed, indicating that there is no predominant wavevector in those surfaces. The dashed line used by Yang et al. (2016) to mark the onset scale

for surface roughness, i.e. where it is assumed that there is no influence of the local shape, is also shown. Figure 7 illustrates how to determine the location of the dashed line based on surface area, where the surface area is approximated using the method of Clarke (1986) in which surface area of a certain grid size is divided into four triangular prisms. As seen in the figure, the surface area increases as the grid size becomes smaller, while a coarser grid leads to highly fluctuating values of the surface area. At the grid size of approximately 0.18 μm the surface area starts to increase significantly, which has been interpreted as asperities of surface roughness enter the surface area estimation for those small grid sizes (Yang et al., 2016).

3.3 Bridging the surface measurements by μCT and interferometer

The surface measurements from the μCT and interferometer result in closed and open surfaces, respectively, leading to different power spectra as shown in figure 2 and figure 4. In order to consider the two separate measurements in a unified framework, we refer to results from Chevrot et al. (1998) who found, based on research on earth dynamics, that when the power spectrum based on Fourier transform (eg. Eq. (8)) is per unit surface, the power spectrum is comparable to that from Eq. (5) for a closed surface. Chevrot (1998) showed that after angular averaging, the PSD of a local surface height can be expressed as:

$$PSD(k) = \frac{2\pi}{16\left(N_x N_y\right)^2 kr} \Im\left|2\mathrm{D}FFT\right|^2 \tag{11}$$

Combined with Eqs. (8) and (9), a factor of $(2\pi)^3/16Akr$ is obtained and therefore applied to the power spectrum from Eq. (8). By using the Jean's rule (Jean, 1932), the wavenumber, *k*, can be related to the harmonic angular degree, *l*, through:

$$k = \frac{\sqrt{l(l+1)}}{r} = \frac{l+0.5}{r}(l >> 1) \tag{12}$$

where *r* is given by Eq. (3). This relation has been widely used in seismic research (e.g. Anderson and Toksoz, 1963; Simons et al., 2006). Jean (1932) pointed out that oscillation under its natural frequency or free oscillation can be regarded as the superposition of traveling waves on the earth surfaces. Physically, an integral number of asymptotic wavelengths are fitted within the cap of radius *r*.

As indicated by Eq. (12), to rebuild the particle shape to the same scale the maximal harmonic degree required would vary for different particle sizes. The maximal harmonic degree is a key parameter to rebuild particle shape. This parameter however does not provide direct information on scales, which may lead to the different suggestions on the maximal harmonic degree that should be used to indicate the limiting scale for particle shape (e.g. Zhou et al., 2015, 2018; Su and Yan, 2018).

Figures 8 and 9 show the resulting PSD for surface measurements at the two different scales in a plot of PSD versus wavenumber for CG and FS, respectively. Several observations can be made:

a) The adopted maximum harmonic degree of 18 corresponds to a wavenumber of approximately 25 mm^{-1} or a wavelength of approximately 0.25 mm (=2π/wavenumber) for particle sizes of 1.18~2 mm, which is much larger than has been achieved in the μCT (around 0.016 mm). This indicates that surface details have been

removed during the approximation of the particle surface with spherical harmonic expansions, which is consistent with the observations in figure 6. To approximate the particle surface as detailed as has been scanned in the μCT would require a harmonic degree of more than 350 (through Eq. (12)), which may not be practical for numerical modelling considering a large quantity of soil particles.

b) The surface roughness scale that was determined by Yang et al. (2016) is indicated by the dashed line (with a wavenumber being around 3400 mm^{-1}) in Figure 6. It has a much smaller length scale (around 0.0018 mm) than the resolution of the μCT measurements. Similar scales have been used by e.g. Altuhafi and Coop (2001) and Senetakis et al. (2013) when determining the roughness of sand grain surfaces. The range bounded by the maximal harmonic degree of 18 that is at the same level as in e.g. Zhou et al. (2018) for particle shape reconstruction and the wavevector of 3400 mm^{-1} that was used to define surface roughness is missing in terms of measurements. This missing scale range, which is due to the limitations of the instruments currently used to describe soil grains, also indicates a caveat in the current characterisation and reconstruction of multi-scale particle morphology. Eq. (7), which relates harmonic degree to wavenumber and a radius that is strongly related to particle size, indicates however that a finer scale could be reached for smaller particle sizes when the harmonic degree is kept constant as 18, suggesting that this missing range may disappear for particles with sizes much smaller than 1 mm (such as silt size). In previous studies, which were mostly made on particles of sand size, the existence of a missing range would however be very likely.

c) The average values of PSD from μCT and interferometer are also shown in the figure as lines with circle markers. Best fit lines, denoted by the bolded dashed lines, are made to the two average lines. It is seen that the slopes are very similar as indicated

by the slopes of best fit lines with r^2 value being more than 0.98 for CG particles of two size ranges (Figure 8). This suggests that a single fractal scaling could apply across the scale spanning from particle shape to surface texture scale. For FS particles (Fig. 9) however, the data suggest different power laws at different scales.

The power spectrum analysis applied to μCT and interferometer measurements on a given soil reveals that different power law patterns can emerge for different soils, here for CG and FS particles. By superposing the PSD components at each different wavenumber, the multi-scale morphology of the soil grains is obtained. Here, the unique power law found for CG particles (Figure 8) indicates a self-affine pattern for the particle surface at different scales, which may be attributed to the random crushing process, resulting in a surface pattern that is repeated at smaller scales. The fact that particles of 1.18~ 2 mm and smaller sizes could exist as single minerals (e.g. biotite, feldspar or quartz), thus with different hardness and fracture surfaces, reinforces the hypothesis that the self-similar nature of the surface of the freshly crushed granite may be due to the random process with which it was created. On the other hand, for the FS particles (Fig. 9) different power law patterns are shown at different scales. The FS is formed by long-term physical weathering process, leading to changes of the particle morphology at different scales i.e. chipping of particle corners, abrasion of the surface, surface erosion etc. The resulting different power law patterns at different scales indicate that the fractal dimension at large scale (as from μCT) cannot simply be extended to smaller scales for this natural sand.The PSD is further analysed below using the fractal theory.

4. Fractal analysis of the multi-scale morphology

The fractal approach (Persson et al., 2005; Yang et al., 2016) was adopted with a minor modification to the exponent so that it could be applied to the measurements from both interferometer and μCT, through

$$PSD(k \geq k_c) = C_0 \left(\frac{k}{k_c} \right)^{\alpha - 1} \tag{13}$$

where $\alpha\ (< 0) = 2D - 8$ is adopted and k_c denotes the onset wavevector of fractal scaling. Note that the PSD here is per unit surface. The addition of minus one accounts for the correction factor applied to Eq. (8); a similar approach could be found in Turcotte (1997). When combined with Eq.(13), Eq. (7) can also be expressed in terms of fractal parameters, C_0 and D (Power and Tullis, 1997), as:

$$S_q(k \geq k_c) = \sqrt{\frac{k_c C_0 r_{00}}{\alpha} \left[\left(\frac{k}{k_c} \right)^{\alpha} - 1 \right]} \tag{14}$$

The fractal dimension is then calculated for each μCT and interferometer measurement. Table 1 shows the statistics of fractal dimensions for the two tested sands at two particle sizes. For CG particles, as also indicated from figure 8, the fractal dimension between μCT and interferometer measurements is consistent considering the standard deviation of μCT measurements (STD). A single fractal dimension for both particle shape and surface texture scales from approximately 2 mm down to approximately 0.2 μm may therefore be assumed, ranging from 2.39 to 2.44, though larger particles tend to have a slightly larger value of D. Compared to CG particles, different power law patterns (and

thus different values of *D*) for the μCT and interferometer measurements are found for FS particles. The fractal dimension *D*, which is expected to be between 2 and 3 for three-dimensional situations, is slightly smaller than 2 for the size range of 1.18~2 mm, as it was determined from the whole scale range of μCT measurements, and may include both shape and surface texture scales for FS particles (as indicated in figure 9). In addition, because the power spectrum curves for μCT measurements are determined at discrete points, they tend to fluctuate, especially at smaller wavenumbers or harmonic degree (as in Fig. 4 and Fig. 9). The larger fractal dimensions describing the roughness of the CG particles may also be due to their more angular shape compared to FS particles that are mostly sub-rounded: The angular edges may be regarded as large-size asperities on the surface, the more angular particles thus are abundant with large-size asperities leading to more uneven surfaces. From the fractal analysis of interferometer measurements, it is found that at that smaller scale CG particles have smaller values of *D* than FS particles, and thus smoother surfaces. A possible reason is that the FS particles underwent more surface changes, whereas the surfaces of CG particles are relatively freshly created, and can include cleavage planes. This is consistent with previous observations (i.e. Anbeek, 1992) that freshly created surfaces are in general smoother than naturally weathered surfaces.

Table 1. Statistics of the fractal dimensions for the two tested sands

Measurements \ Particle size, mm		CG		FS	
		0.6-1.18	1.18-2	0.6-1.18	1.18-2
μCT	Mean	2.39	2.44	2.16	1.92
	STD	0.13	0.13	0.18	0.32
Interferometer	Mean	2.42	2.42	2.45	2.47
	STD	0.05	0.05	0.04	0.03

To rebuild a surface with multi-scale morphology as detailed as examined by the interferometer, using the spherical harmonic method alone would require a harmonic function at a degree of more than 300. As this cannot be easily achieved, here it is proposed to rebuild the surface on the particle shape built to a harmonic degree that can be easily achieved, and by superimposing remaining surface features which can be represented by a roughness measurement and fractal parameters. The surface roughness is represented by the S_q value, which has been adopted in numerical modelling (Yimsiri and Soga, 2000; Scharinger et al., 2008 and Otsubo et al., 2015) and which, when obtained from power spectrum analysis, has been shown to be in excellent (error <0.1%) agreement with the value from the equation defining the S_q (Yang et al., 2016). In those previous works, the S_q value was based on local measurements. If we call S_{q_real} the S_q value obtained from μCT measurements, S_{q_real} is defined as:

$$S_{q,\,\text{real}} = \sqrt{\frac{1}{M}\sum_{i=1}^{m}\left(r_i - r_{00}\right)^2} \tag{15}$$

where r_i is the radius of the particle scanned from μCT and M is the number of vertices. The average value of r is the base line and is taken as the value of r_{00}. Here the approximated S_q comprises that from the shape and from the surface texture, which are given, respectively, as:

$$S_{q,\,\text{shape}} = \sqrt{\frac{1}{M}\sum_{i=1}^{m}\left(r_{i,\text{shape}} - r_{00}\right)^2}$$

where $r_{,\text{shape}}$ is the radius of the particle reconstructed at SH of 10 for example, and

$$S_{q,\,\text{surface texture}} = \sqrt{\frac{k_c C_0 r_{00}}{\alpha}\left[\left(\frac{k}{k_c}\right)^{\alpha} - 1\right]}$$

where k_c=(SH+0.5)/r_{00} and k=π/voxel size of μCT images.

If we compare the proposed method with the roughness directly measured from μCT measurements:

$$S_{q,\,\mathrm{real}}{}^{2} = S_{q,\,\mathrm{shape}}{}^{2} + S_{q,\,\mathrm{surface\ texture}}{}^{2} \tag{16}$$

We find (see figure 10) that the proposed method at SH of 10 gives a S_q value that agrees well (5% error) with that from experiments (Eq. (11)). The choice of the SH of 10 is rather arbitrary, but can broadly be justified by considering that the volume of the rebuilt particle is almost (within 5% error) as scanned (Fig. 4). Other SHs may also be used. As seen in figure 11, the errors become smaller as the particle shape is reconstructed at larger SHs. When an error of 15% is considered acceptable, a SH of 4 can also be used, which reduces the time to rebuild the particle shape.

Figure 12 shows a particle shape reconstructed at a harmonic degree of 10, corresponding to a length scale being around 0.5 mm for CG particles between 1.18~2 mm, with a surface texture corresponding to harmonic degrees larger than 10 (corresponding to a wavenumber of 12.3 mm^{-1}) which are represented by fractal parameters (C_0=4.55e-5 mm^2, D=2.41) obtained from the interferometer measurements. The reconstructed particle has a roughness S_q of 13.2 μm, calculated based on the equation for global surface roughness. In this way, the particle as measured by the μCT and interferometer is translated to the particle shape reconstructed to the harmonic degree of 10 and the surface texture represented by fractal parameters. Here, the single fractal dimension has facilitated the conversion of the surface measurements into numerically constructed particles, but it is not necessarily a prerequisite.

For the FS particles, the existence of more than one power law highlights the need for a separation scale between particle shape and surface texture. In the proposed method, the surface texture comprises of surface roughness and local curvature which

relates to the missing range (denoted in figures 8 and 9). The onset scale for the local curvature or surface texture acts thus as a separation scale. Orford and Whalley, (1987) suggested that when more fractal subsets are found, they could be used to describe different morphological scales. Determined from the cross points between the PSD from micro CT and interferometer measurements (Fig. 9), the separation scales can roughly be estimated as from 0.003 to 0.79 mm for sizes of 0.6~1.18 mm and 0.03 to 1.57 mm for sizes of 1.18~2 mm, and delineate two distinct fractal domains. In the case of CG particles, the single fractal dimension renders the identification of a boundary between particle shape and surface texture not straightforward. When taking into account both the particle volume of reconstructed particle relative to a scanned particle and the error in S_q, the separation scale for CG might be considered at the SH of 10 corresponding to a wavenumber of around 13 mm^{-1} for 1.18 ~2 mm and around 23 mm^{-1} for 0.6~1.18 mm.

5. Conclusion

The multi-scale morphology of sand has been analysed with the aid of power spectrum, applied at both the particle shape scale as examined by μCT or the scale of the surface texture determined by interferometer. A missing scale range in the current characterisation of particle morphology has been identified, related to the limitations of current technology. To bridge the missing scale, the fractal analysis offers an alternative to rebuild a particle surface at multi-scale morphology. Here we proposed to rebuild the surface at particle shape scale to a harmonic degree that can be easily achieved, and by considering the rest of the surface features as the surface texture scale which can be represented by fractal parameters determined from interferometer measurements.

The proposed method, applied to a freshly crushed granite made of angular grains (CG), and natural Fujian sand made of mostly sub-rounded particles (FS), both of sizes 0.6 mm to 2 mm, highlights the importance of the soil's history on its morphology. In FS sands, different self-affine patterns at different scales are present, of which the cross-point can be regarded as a separation between shape and surface texture. This also implies that for this natural sand, extrapolation of the self-affine pattern observed at large scales to small scales may not be valid. For CG particles, a unique self-affine pattern is found applicable to a length scale from approximately 2 mm down to approximately 0.2 μm. The single self-pattern possibly arises from the random crushing process and may be a favourable element for modelling at particle scale as it shows that the same fractal dimension can be used to describe the shape and surface texture, thus measurements based on the larger-scale morphology can be extended to the smaller scale. The separation between shape and surface texture is not straightforward but can be indicated with considerations of the volume of rebuilt particles and root-square value of surface heights.

Although the current analysis was developed for star-shaped particles, it gives some insight into the multi-scale morphology of soil particles and how the scales of surface texture and of particle shape are related. Characterising the morphology of soil grains within a single framework across scales also serves the purpose of allowing precise replica particles to be created, either by way of 3D printing or for use in DEM.

Acknowledgements

HY thanks Mr. Yanlu Ding and Dr. Wei LI for the assistance with micro CT measurements at the University of Hong Kong, and Dr. Ting Yao for discussion with interferometer measurements. Financial support provided by the Research Grants Council of HKSAR (TR22-603-15N) and by the German Science Foundation (DFG) in

the framework of the Collaborative Research Centre SFB 837 “Interaction modeling in Mechanized Tunnelling” is acknowledged. The constructive comments from the two anonymous reviewers improve the scientific contribution and readability of the manuscript and are also greatly acknowledged.

References

Anbeek C (1992) Surface roughness of minerals and implication for dissolution studies. Geochimica et Cosmochima Acta 56(4):1461–1469

Alshibli KA, Druckrey AM, Ai-Raoush RI, Weiskittel T and Lavrik NV (2014) Quantifying Morphology of Sands Using 3D Imaging. *Journal of Materials in Civil Engineering* **27(10)**: 04014275.

Altuhafi F and Coop M (2011) Changes to particle characteristics associated with the compression of sands. *Géotechnique* **61(6)**: 459–471

Anderson DL and Toksöz MN (1963) Surface waves on a spherical Earth: 1. Upper mantle structure from Love waves. Journal of Geophysical Research. 68(11):3483-500.

Bills BG and Kobrick M (1985) Venus topography: A harmonic analysis. *Journal of Geophysical Research: Solid Earth* ***90*****(B1)**, 827-836.

Bowman ET, Soga K and Drummnond W (2001) Particle shape characterisation using Fourier descriptor analysis. *Geotechnique* 51(6): 545–554.

Carrier III WD (2003) Goodbye, hazen; hello, kozeny-carman. *Journal of Geotechnical and Geoenvironmental Engineering* **129(11)**, 1054-1056.

Cho GC, Dodds J and Santamarina JC (2006) Particle Shape Effects on Packing Density, Stiffness, and Strength: Natural and Crushed Sands. *Journal of Geotechnical and Geoenvironmental Engineering* ***132*****(5):** 591-602.

Chevrot S, Montagner JP and Snieder R (1998) The spectrum of tomographic earth models. *Geophysical Journal International* ***133*****(3)**, 783-788.

Clarke KC (1986) Computation of the fractal dimension of topographic surfaces using the triangular prism surface area method. Comput. Geosci. 12, 713–722.

Ehrlich R and Weinberg B (1970) An exact method for characterisation of grain shape, *Journal of Sedimentary Research* **40**: 205-212.

Fonseca J, O'Sullivan C, Coop MR and Lee PD (2012) Non-invasive characterisation of particle morphology of natural sands. *Soils and Foundations* **52(4):** 712-722.

Garboczi EJ (2002) Three-dimensional mathematical analysis of particle shape using X-ray tomography and spherical harmonics: Application to aggregates used in concrete. *Cement and concrete research* ***32*****(10):** 1621-1638.

Geotechnical Engineering Office (GEO) (2017). Guide to Rock and Soil Descriptions (Geoguide 3), Civil Engineering and Development Department, HKSAR Government.

Gonzalez RC and Woods RE (2010) Digital Image Processing, Pearson/Prentice Hall, Upper Saddle River, N.J., 2010

Jeans JH (1923) The propagation of earthquake waves. *Proceedings of the Royal Society of London a Mathematical, Physical and Engineering Sciences* ***102*****(718):** 554-574.

Kaula WM (1967) Theory of statistical analysis of data distributed over a sphere. *Reviews of Geophysics* ***5*****(1):** 83-107.

Kawamoto R, Andò E, Viggiani G and Andrade JE (2016) Level set discrete element method for three-dimensional computations with triaxial case study. *Journal of the Mechanics and Physics of Solids* **91:** 1-13.

Matsushima T and Chang CS (2011) Quantitative evaluation of the effect of irregularly shaped particles in sheared granular assemblies. *Granular Matter* **13(3)**: 269–276.

Mollon G and Zhao J (2013) Generating realistic 3D sand particles using Fourier descriptors. *Granular Matter* ***15*(1):** 95-108.

Nayak PR (1971) Random process model of rough surfaces. *Journal of Lubrication Technology* **93**: 398–407

Persson BJN, Albohr O, Tartaglino U, Volokitin AI and Tosatti E (2005) On the nature of surface roughness with application to contact mechanics, sealing, rubber friction and adhesion. *Journal of Physics: Condensed Matter* **17**: R1–R62.

Power WL and Tullis TE (1991) Euclidean and fractal models for the description of rock surface roughness. *Journal of Geophysical Research-Solid Earth* **96(B1)**: 415-424.

Orford JD and Whalley WB (1987) The quantitative description of highly irregular sedimentary particles: the use of the fractal dimension. In Clastic particles. Scanning electron microscopy and shape analysis of sedimentary and volcanic clasts (ed. JR Marshall), pp. 267–280. New York, NY: Van Nostrand Reinhold Co.

Otsu N (1979) A threshold selection method from gray level histograms. IEEE Transactions on Systems, Man and Cybernetics 9, 62–66.

Otsubo M, O'Sullivan C, Sim WW and Ibraim E (2015) Quantitative assessment of the influence of surface roughness on soil stiffness. *Géotechnique* **65(8)**: 694–700.

Rasband WS (1997–2011). ImageJ, U. S. National Institutes of Health, Bethesda, Maryland, USA.

Sandeep CS, He H and Senetakis K (2018) An experimental micromechanical study of sand grain contacts behavior from different geological environments. *Engineering Geology* **246**: 176-186.

Senetakis K, Coop MR and Todisco MC (2013) The inter-particle coefficient of friction at the contacts of Leighton Buzzard sand quartz minerals. *Soils and Foundations* **53(5):** 746-755.

Simons FJ, Dahlen FA and Wieczorek MA (2006). Spatiospectral concentration on a sphere. SIAM review, 48(3), 504-536.

Szerakowska S, Woronko B, Sulewska, MJ, Oczeretko, E. 2018. Spectral method as a tool to examine microtextures of quartz sand-sized grains. Micron, 110, 36-45.

Turcotte DL (1997) Fractals and chaos in geology and geophysics. Cambridge, UK: Cambridge University Press

Wieczorek MA and Simons FJ (2005) Localized spectral analysis on the sphere. *Geophysical Journal International* ***162*(3):** 655-675.

Wieczorek MA (2015) Gravity and topography of the terrestrial planets. *Treatise on Geophysics* ***10*(257)**: 153-193.

Yang H, Khoshghalb A, and Russell AR (2014) Fractal-based estimation of hydraulic conductivity from soil-water characteristic curves considering hysteresis. *Geotechnique letters* **4(1)**: 1-10.

Yang H, Baudet BA and Yao T (2016) Characterisation of the surface roughness of sand particles using an advanced fractal approach. *Proceedings of the Royal Society of London a Mathematical, Physical and Engineering Sciences* **472**: 20160524.

Yang HW, Lourenco SND., Baudet BA, Choi CE and Ng CW (2019) 3D Analysis of gravel surface texture. *Powder Technology* **346**:414-424.

Yang J and Luo XD (2015) Exploring the relationship between critical state and particle shape for granular materials. *Journal of the Mechanics and Physics of Solids* ***84:*** 196-213.

Yao T, Baudet BA and Lourenço SDN (2018) Quantification of the surface roughness of quartz sand using optical interferometry. *Meccanica* : 1-8.

Zhou B, Wang J and Zhao B (2015) Micromorphology characterisation and reconstruction of sand particles using micro X-ray tomography and spherical harmonics. *Engineering geology* **184**: 126-137.

Zhou B and J. Wang J (2017) Generation of a realistic 3D sand assembly using X-ray microcomputed tomography and spherical harmonic-based principal component analysis, International Journal for Numerical and Analytical Methods in Geomechanics 41 93–109.

Zhou B, Wang J and Wang H (2018) Three-dimensional sphericity, roundness and fractal dimension of sand particles, *Géotechnique* **68 (1)**: 18–30.

Zhao BD and Wang JF (2016) 3D quantitative shape analysis on form, roundness, and compactness with μCT, *Powder Technology* **291**: 262–275.

List of notation

2DFFT	two-dimensional discrete Fourier transform
A	projection area of surface heights $h(x, y)$
A_i,B_i,C_i	vertices of the ith triangular face of the surface mesh
C_0	fractal parameter related to the intercept of the straight line in double logarithmic plane
D	fractal dimension
N	maximal degree of the SH function
N_x, N_y	data points on the x and y direction
PSD	power spectrum
P_l^m	an associated Legendre function
O	centre of particle
SA	surface area of reconstructed particle
SH	spherical harmonics
V	volume of reconstructed particle
a	the resolution on the x-y plane
f_{lm}	corresponding SH expansion coefficient
$h(x, y)$	surface heights
k, k_x, k_y	wavenumber, wavenumber along x and y axis
k_c	onset wavevector of fractal scaling
l	harmonic degree
m	order of harmonic degree
$r(\theta, \varphi)$	polar radius or the distance from the origin that is located inside a particle to each point on the original particle surface

r_{00}	the radius of the sphere at 0 degree and 0 order
S_q	root-mean-square value of surface height
$S_{q,\,\mathrm{real}}$	S_q value obtained from μCT measurements
$S_{q,\,\mathrm{shape}}$, $S_{q,\,\mathrm{surface\ texture}}$	S_q comprises that from shape and surface texture
Y_l^m	spherical harmonic of degree l and order m
α	exponent in Eq.(13)
θ	polar angle, [0, π]
φ	azimuthal angle, [0, 2π]
$\Im$	angular averaging

Table 2. Statistics of the fractal dimensions for the two tested sands

Measurements	Particle size, mm	CG		FS	
		0.6-1.18	1.18-2	0.6-1.18	1.18-2
μCT	Mean	2.39	2.44	2.16	1.92
	STD	0.13	0.13	0.18	0.32
Interferometer	Mean	2.42	2.42	2.45	2.47
	STD	0.05	0.05	0.04	0.03

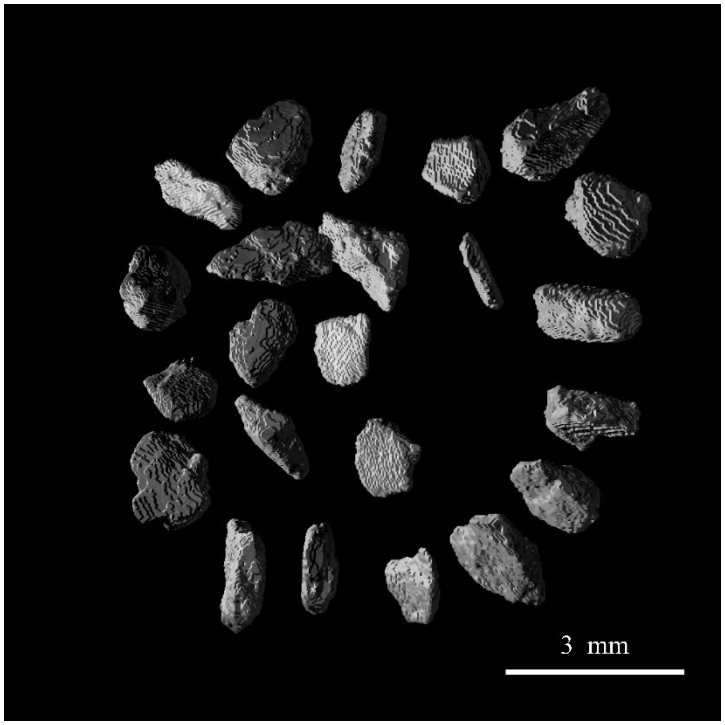

(a)

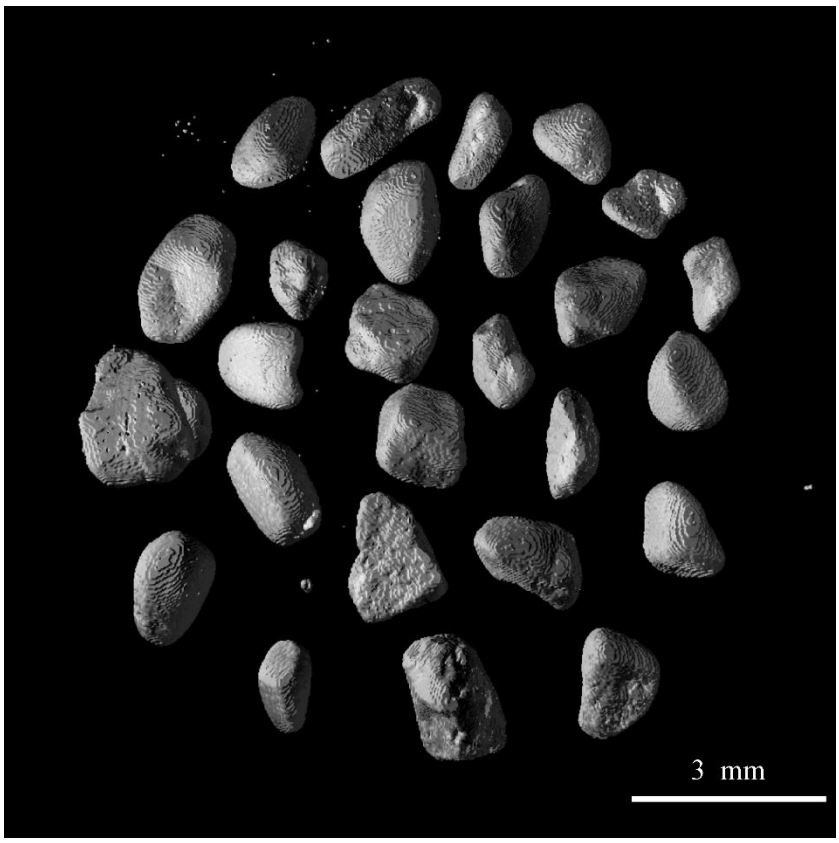

(b)

Figure 1. Voxel assemblage of a) CG sand particles and b) FS particles

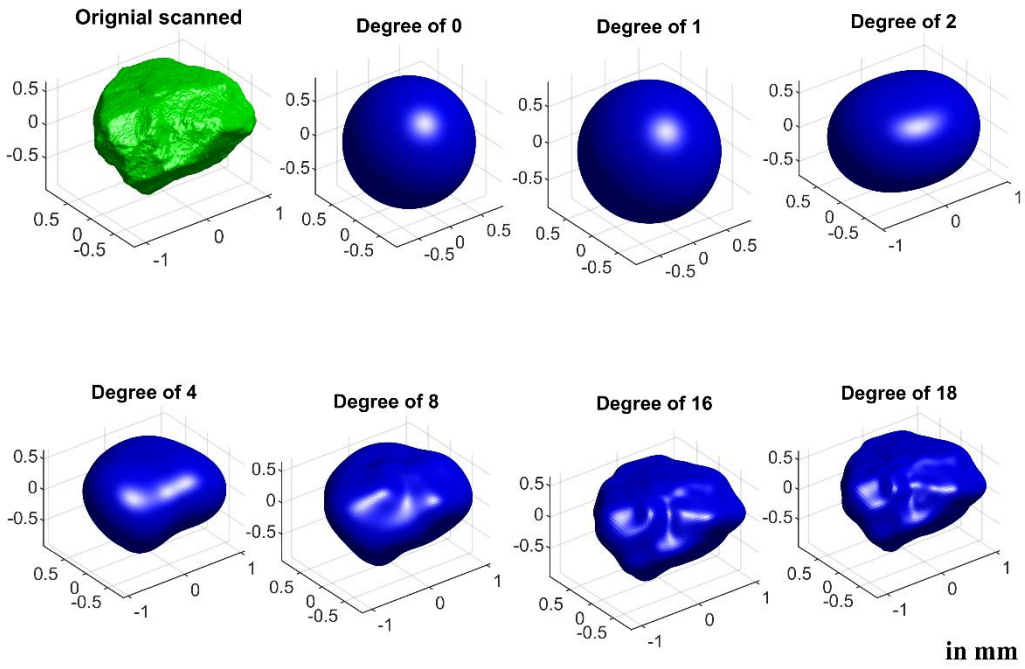

Figure 2. Particle shape reconstructed at different harmonic degrees

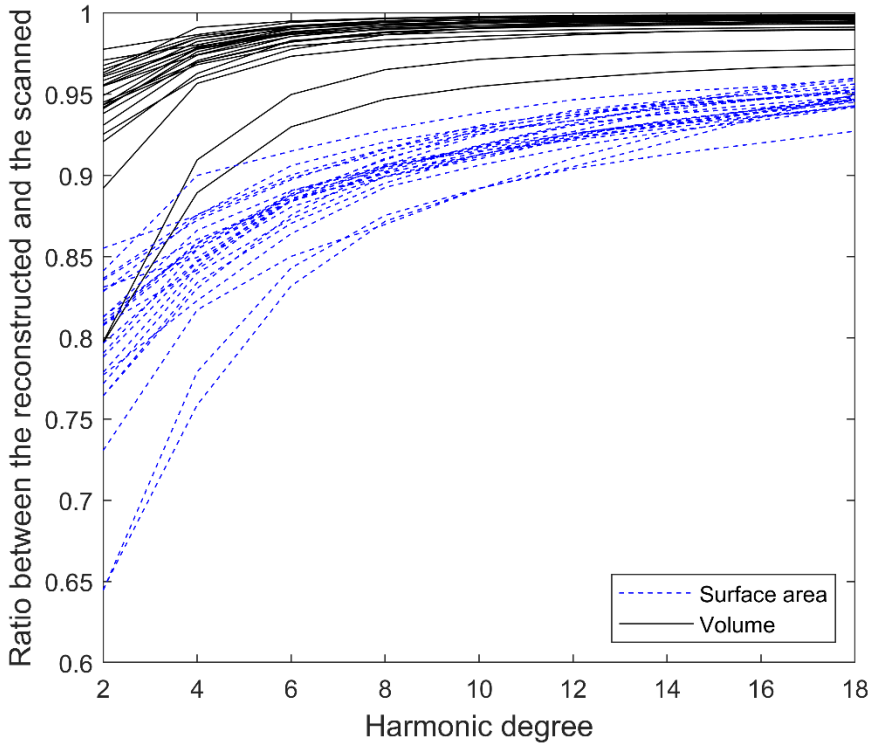

Figure 3. The ratio of surface area and volume between the reconstructed particle and the scanned particle from micro CT in the ratio versus harmonic degree plane. Results are for some of the scanned particles.

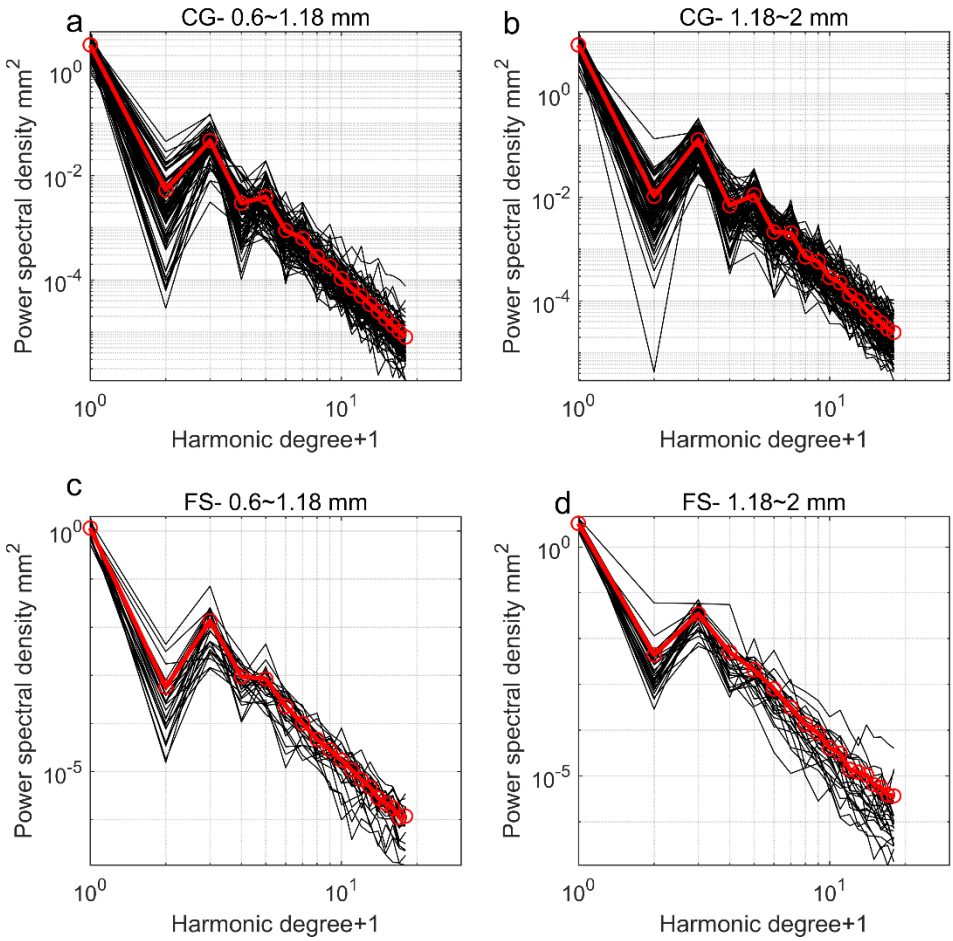

Figure 4. Power spectrum of µCT measurements in PSD vs harmonic degree plane for CG particles at size of a) 0.6~1.18 mm and b) 1.18~2 mm and FS particles at size of c) 0.6~1.18 mm and d) 1.18~2 mm

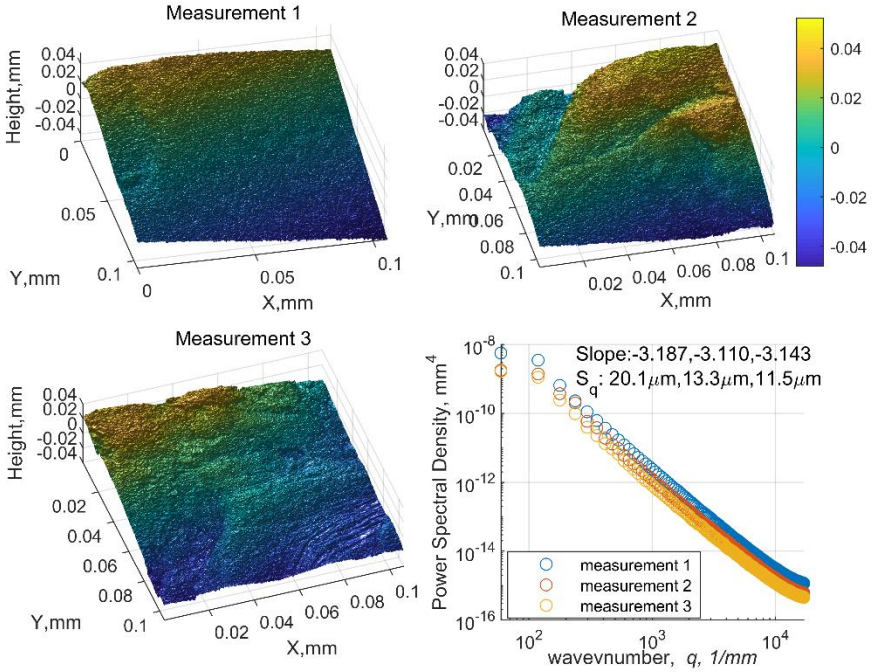
Measurement 1
Measurement 2
Measurement 3
Height,mm
X,mm
Y,mm
Slope:-3.187,-3.110,-3.143
S_q: 20.1μm,13.3μm,11.5μm
Power Spectral Density, mm^4
wavevnumber, q, 1/mm
measurement 1
measurement 2
measurement 3

(a)

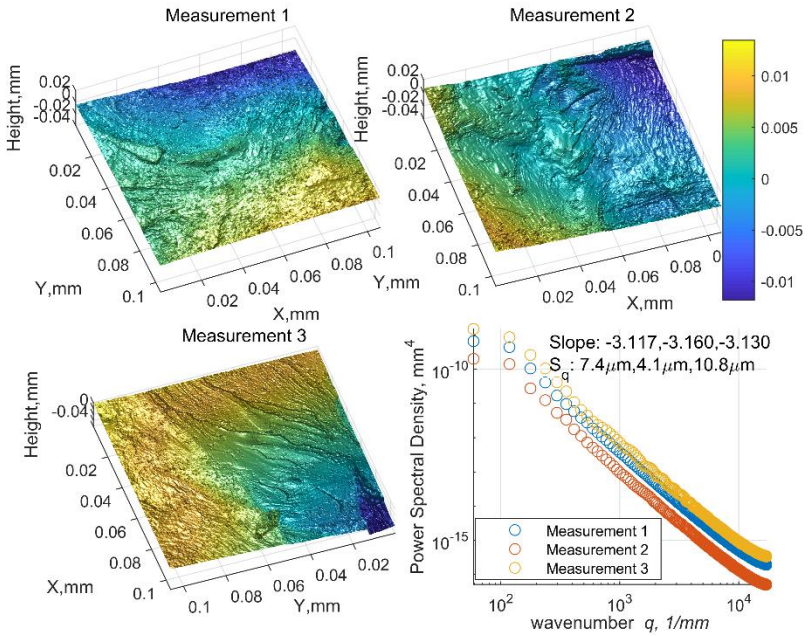
Measurement 1
Measurement 2
Measurement 3
Height,mm
X,mm
Y,mm
Slope: -3.117,-3.160,-3.130
S_q: 7.4μm,4.1μm,10.8μm
Power Spectral Density, mm^4
wavenumber q, 1/mm
Measurement 1
Measurement 2
Measurement 3

(b)

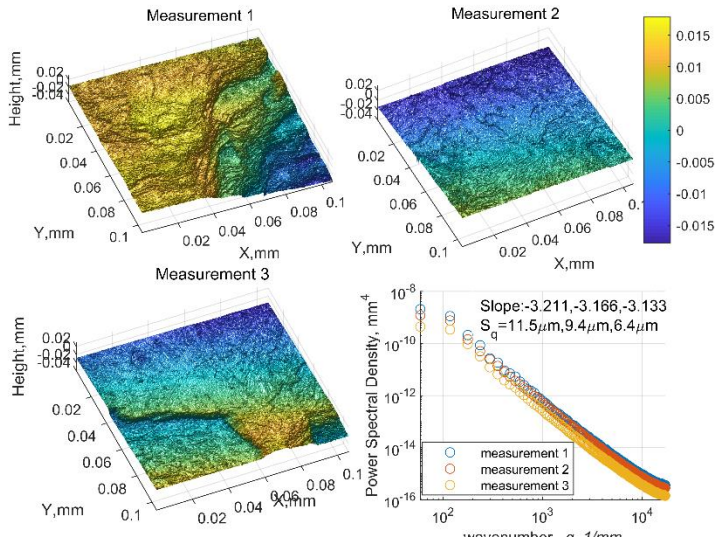

(c)

Figure 5. Surface measurements at three different locations on each particle together with its associated power spectrum for three particles (a-c)

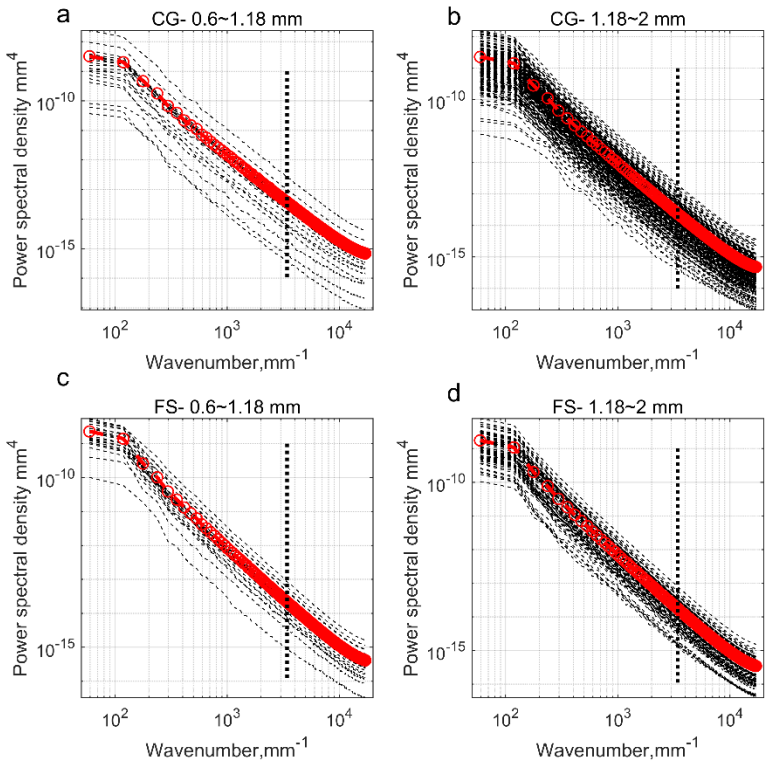

Figure 6. Power spectrum of interferometer measurements in the PSD vs wavenumber plane for CG particles at sizes of a) 0.6~1.18 mm and b) 1.18~2 mm and FS particles at sizes of c) 0.6~1.18 mm and d) 1.18~2 mm. The dotted line is the separation line for surface roughness. Open circles are average values.

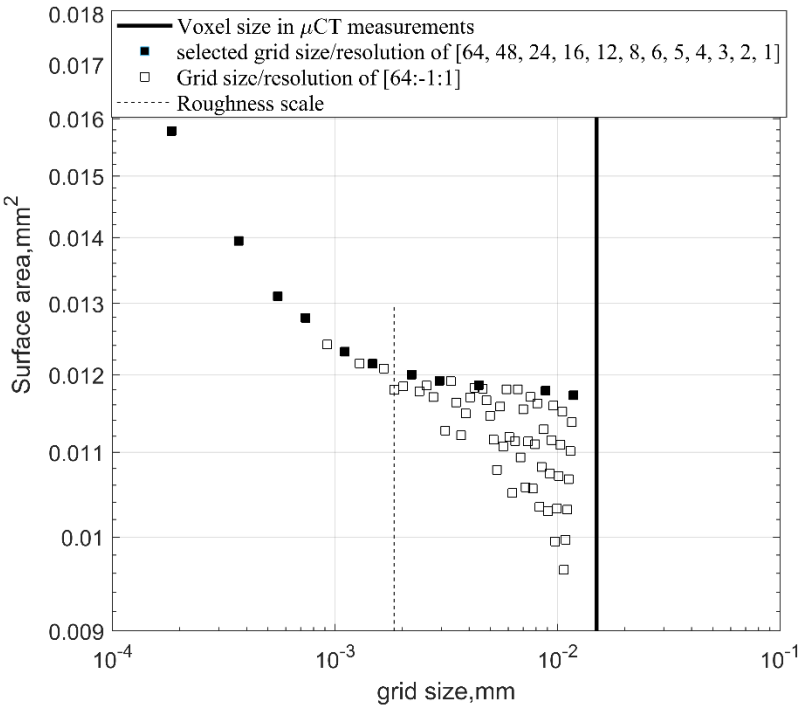

Figure 7. Estimated surface area for grid sizes of [64, 48, 24, 16, 12, 10, 8, 6, 5, 4, 3, 2, 1] × 0.184 μm and finer discretization [64: -1: 1] × 0.184 μm on a measuring area of 0.106×0.106 mm.

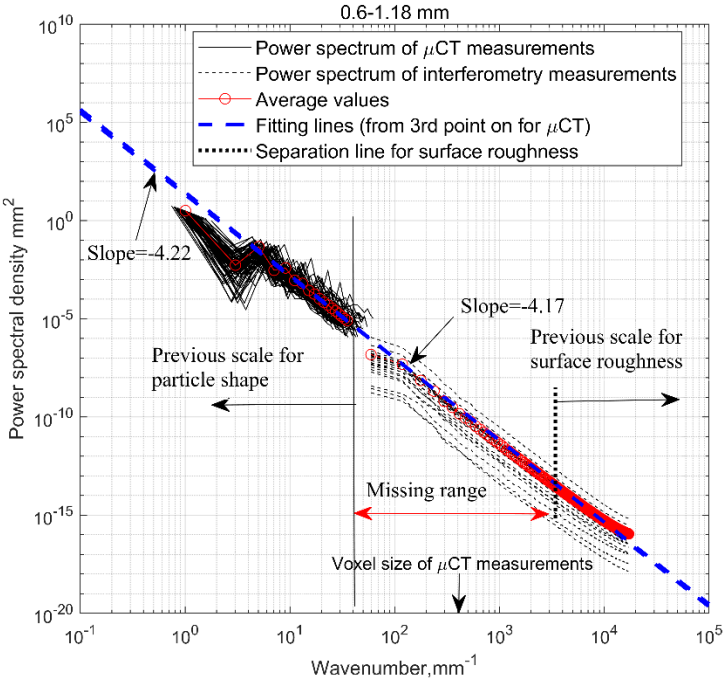

(a)

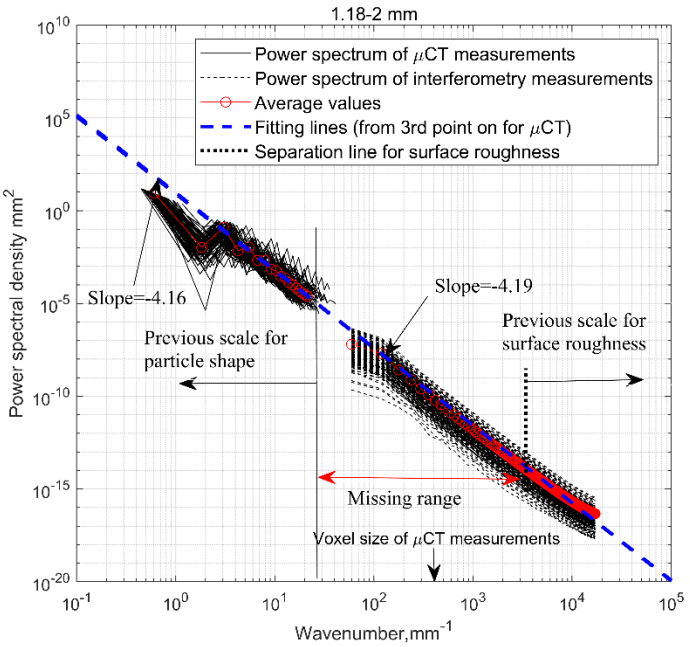

(b)

Figure 8. Power spectrum of both μCT and interferometer measurements versus wavenumber for CG particles at size range of a) 0.6~1.18 mm and b) 1.18~ 2 mm. The dotted line indicates the scale separating local curvature and roughness as adopted from Yang et al. (2016). The thick dashed line for μCT measurements is fitted from around the third point on.

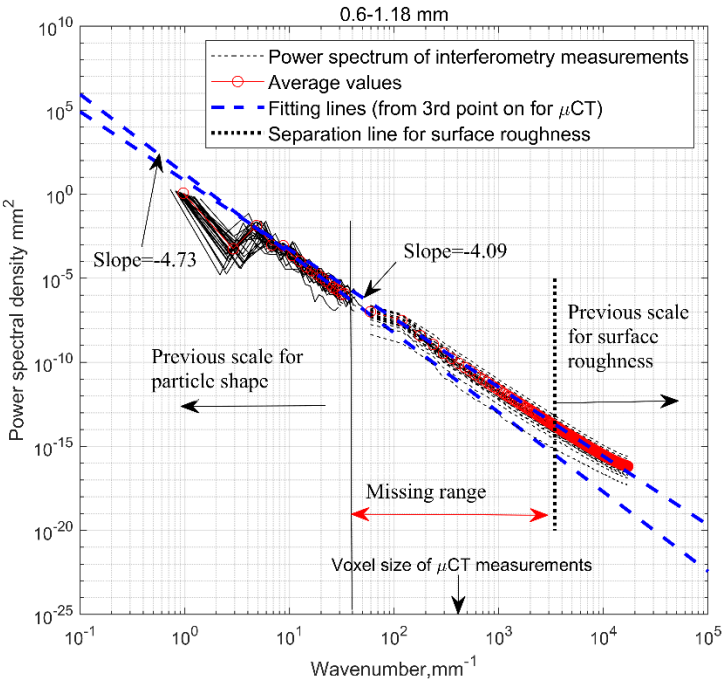

(a)

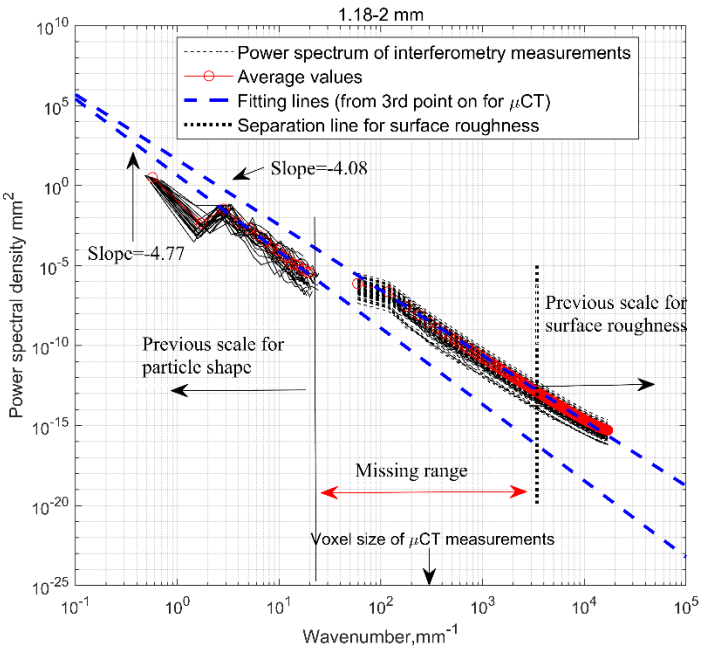

(b)

Figure 9. Power spectrum of both μCT and interferometer measurements versus wavenumber for FS particles at size range of a) 0.6~1.18 mm and b) 1.18~ 2 mm

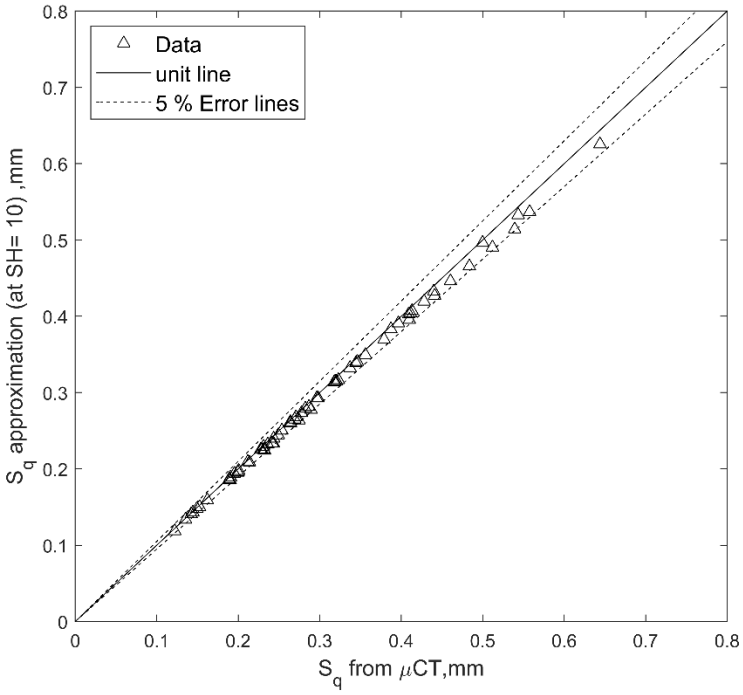

Figure 10. Comparison of S_q value from proposed method at SH of 10 with that from statistics

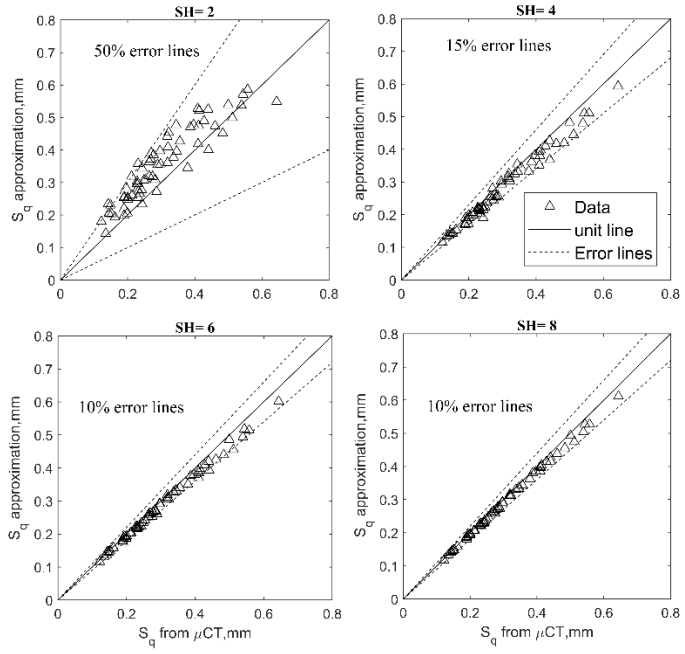

Figure 11. Comparison of S_q value from proposed method at SH of 2, 4, 6 and 8 with that from statistics

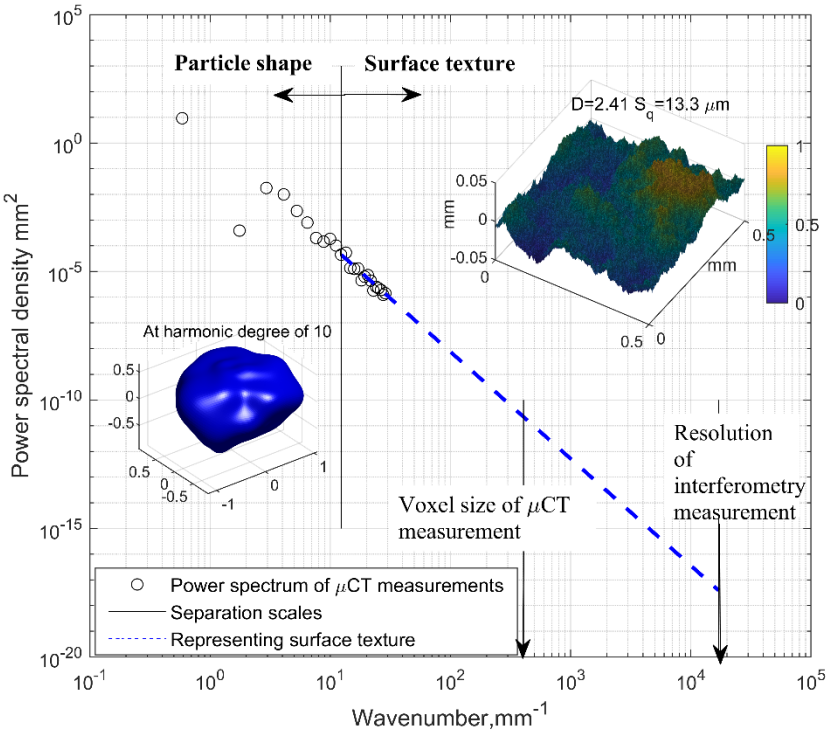

Figure 12. Separation between particle shape and surface texture at a particular harmonic degree